nanomaterials

MDPI

Article

Copper Nanowires as Highly Efficient and Recyclable Catalyst for Rapid Hydrogen Generation from Hydrolysis of Sodium Borohydride

Aina Shasha Hashimi [1], Muhammad Amirul Nazhif Mohd Nohan [1], Siew Xian Chin [2], Poi Sim Khiew [3], Sarani Zakaria [1] and Chin Hua Chia [1,*]

1 Materials Science Program, Department of Applied Physics, Faculty of Science and Technology, Universiti Kebangsaan Malaysia, Bangi 43600, Selangor, Malaysia; aina1shasha@gmail.com (A.S.H.); nazhifamirul@gmail.com (M.A.N.M.N.); szakaria@ukm.edu.my (S.Z.)

2 ASASIpintar Program, Pusat GENIUS@Pintar Negara, Universiti Kebangsaan Malaysia, Bangi 43600, Selangor, Malaysia; chinsiewxian@ukm.edu.my

3 Center of Nanotechnology and Advanced Materials, Faculty of Engineering, University of Nottingham Malaysia Campus, Jalan Broga, Semenyih 43500, Selangor, Malaysia; PoiSim.Khiew@nottingham.edu.my

* Correspondence: chia@ukm.edu.my; Tel.: +603-8921-5473

Received: 27 May 2020; Accepted: 10 June 2020; Published: 12 June 2020

Abstract: Hydrogen (H_2) is a clean energy carrier which can help to solve environmental issues with the depletion of fossil fuels. Sodium borohydride ($NaBH_4$) is a promising candidate material for solid state hydrogen storage due to its huge hydrogen storage capacity and nontoxicity. However, the hydrolysis of $NaBH_4$ usually requires expensive noble metal catalysts for a high H_2 generation rate (HGR). Here, we synthesized high-aspect ratio copper nanowires (CuNWs) using a hydrothermal method and used them as the catalyst for the hydrolysis of $NaBH_4$ to produce H_2. The catalytic H_2 generation demonstrated that 0.1 ng of CuNWs could achieve the highest volume of H_2 gas in 240 min. The as-prepared CuNWs exhibited remarkable catalytic performance: the HGR of this study (2.7×10^{10} mL min^{-1} g^{-1}) is ~3.27×10^7 times higher than a previous study on a Cu-based catalyst. Furthermore, a low activation energy (E_a) of 42.48 kJ mol^{-1} was calculated. Next, the retreated CuNWs showed an outstanding and stable performance for five consecutive cycles. Moreover, consistent catalytic activity was observed when the same CuNWs strip was used for four consecutive weeks. Based on the results obtained, we have shown that CuNWs can be a plausible candidate for the replacement of a costly catalyst for H_2 generation.

Keywords: acetic acid; catalytic activity; energy efficiency; H_2 spillover; metal nanowires; $NaBH_4$

1. Introduction

Lately, many researchers have been exploring the use of metal nanocrystals in applications such as catalysis, electrocatalysis, sensor design, antimicrobial materials, and flexible transparent electrodes [1–7]. Nanocoppers (Cu) of one-dimensional shape have received attention due to their high electrical conductivity [8]. Compared with noble metals, Cu is much cheaper and abundant [9], making it an attractive option to replace the highly expensive and scarce noble metals in various applications [10]. Due to their large surface area-to-volume ratio, Cu nanocrystals are progressively studied for catalysis applications such as the reduction of nitrophenols and H_2 generation from the hydrolysis of $NaBH_4$ [11,12].

The excessive consumption of fossil fuels has led to the deterioration of the ecological environment and a severe energy crisis, which in turn has increased the intensity of the search for safe, efficient, and clean energy sources. H_2 is considered as a promising candidate to replace traditional fossil

fuels due to its high energy density (142 MJ kg^{-1}) and renewability, and its environmentally friendly by-product (water) [13,14]. H_2 can be stored physically in liquid form or as a compressed gas. However, due to its low boiling and melting points, the pressure needed for the compression is too high which introduces the risk of leakage and explosion hazard [15]. Therefore, the lack of effectiveness, safety, and low cost of the H_2 carrier limits its commercial availability worldwide [14].

On the other hand, chemically storing H_2 in a solid state medium, such as a metal hydride, is potentially a safer and effective method [15,16]. There are several metal hydrides that have been utilized as chemical sources for H_2 production, including sodium borohydride ($NaBH_4$) [17] and lithium borohydride ($LiBH_4$) [18]. $NaBH_4$ is the most commonly utilized among all other metal hydrides because of its non-flammable and non-toxic nature [15]; it is also easy to be hydrolyzed [19,20], and its reaction product ($NaBO_2$) is recyclable [21]. $NaBH_4$ also exhibits high gravimetric/volumetric H_2 storage capacity (10.8 wt%), which results in a high rate of H_2 production [15,20,22]. One mol of $NaBH_4$ can release 4 mol H_2 gas: $NaBH_4 + 2\ H_2O \rightarrow NaBO_2 + 4\ H_2$ ($\Delta H = -217$ kJ mol^{-1}) [21,23].

However, the hydrolysis of $NaBH_4$ is slow at room temperature without a catalyst [24]. Therefore, various catalysts have been employed for the reaction [14,24–27]. Production of pure H_2 can be obtained by the hydrolysis of $NaBH_4$ with a controllable rate at ambient temperature with the presence of an appropriate catalyst. Previous studies showed that noble metals, such as platinum (Pt) [28], ruthenium (Ru) [29], and palladium (Pd) [30], are effective catalysts for the hydrolysis of $NaBH_4$. Even though these catalysts show high stability and excellent catalytic activity, their expensive cost restrains their usage in wide applications [31]. The need to find durable, efficient, and cheap alternatives has led to further research works. Recently, there have been many studies done by using transition metal-based catalysts, such as cobalt [32], nickel [33], manganese [26], and Cu [12], to replace the noble metal catalysts. Some examples of transition metal-based catalysts are graphene-modified Co-B catalysts [14], Ni-Co-B hollow nanospheres [34], and cobalt boride@ nickel/reduced graphene oxide (Co-B@Ni/RGO) nanocomposites [35]. Even though there are many studies related to Cu alloys or composites [36–38], there is only one study reported on the utilization of a Cu-based catalyst for the hydrolysis of $NaBH_4$ [12]. To the best of our knowledge, there has not been any study done as of this moment using CuNWs for the hydrolysis of $NaBH_4$ to generate H_2.

Even though there are advantages to using cheaper transition metals as catalysts, there are still several setbacks: these nanocatalysts are easy to aggregate which leads to a reduction in the specific surface area, thus causing a decrease in catalytic performance [32]. In addition, catalyst regeneration and leaching must also be addressed to increase the life span of the catalyst and availability for practical use. In this study, we synthesized copper nanowires (CuNWs) by a facile hydrothermal route, and we studied its catalytic performance in the hydrolysis of $NaBH_4$ to produce H_2 gas. Additionally, a short and simple treatment using glacial acetic acid (GAA) was conducted on the CuNWs. To avoid aggregation of the CuNWs during the catalytic reaction, the CuNWs were immobilized onto cotton cloth to improve the catalytic performance in terms of reusability, stability, and recoverability.

2. Materials and Methods

2.1. Materials

Copper chloride dihydrate ($CuCl_2$, $2H_2O$, ≥99.0%), octadecylamine (ODA, $C_{18}H_{39}N$, ≥85.0%), sodium borohydride ($NaBH_4$, ≥98%), and chloroform ($CHCl_3$, ≥99.8%) were obtained from Merck. Ascorbic acid (AA, $C_6H_8O_6$, ≥99%) was obtained from Sigma. Glacial acetic acid (GAA, CH_3COOH, 99.85%) was obtained from HmbG Chemicals. Sodium hydroxide (NaOH, 99%) was obtained from SYSTERM. Cotton cloths (CC, 95% cotton) were cut into 0.5 × 1 cm^2 for each hydrolysis reaction. All chemicals were used as received. All solutions were prepared with deionized water.

2.2. Synthesis of CuNWs

CuNWs were synthesized using a hydrothermal approach as reported previous [5]. Briefly, 26.3 mM of ODA, 2.8 mM of AA, and 5.6 mM of $CuCl_2{\cdot}2H_2O$ were dissolved in 30 mL of deionized water under stirring for 10 min and sonicated for 10 min. Next, the solution was transferred into a Teflon-lined autoclave and heated at 120 °C for 20 h. After the synthesis was done, the reddish-brown solution was washed with chloroform to separate CuNWs from other Cu products and kept in a sealed glass vial for further use.

2.3. Preparation of CuNWs Strips Samples

Different loadings of CuNWs (0.1 μg, 0.1 ng, 0.1 pg, and 0.1 fg) were drop-casted on cotton cloth strips (CuNWs/CC) and treated for 10 min using 10% GAA (GAA:isopropyl alcohol = 1:9) by dip coating. The CuNWs strips were kept in a sealed plastic bag and stored in a refrigerator.

2.4. Catalytic Study of H_2 Generation

The kinetic studies of the hydrolysis of $NaBH_4$ were carried out in a batch operation by the water displacement method, where the volume of H_2 gas generated at a given interval is measured by reading the volume of the drained water in the cylindrical tube. In a typical measurement, 10 mL of 1 wt% $NaBH_4$ that has been adjusted to pH 12 was prepared in a rubber sealed 50 mL conical flask. Then, a piece of CuNWs/CC with specific catalyst loading was put into the solution to initiate the catalytic reaction. The catalytic performance of the CuNWs/CC was tested by conducting several experiments at different pHs (10.45, 12, and 13), catalyst loadings (0.1 fg, 0.1 pg, 0.1 ng, and 0.1 μg), $NaBH_4$ concentrations (0.1, 0.5, 1, 3, and 5 wt%), and reaction temperatures (298, 313, 323 and 333 K). Reusability and stability of the CuNWs/CC strips were investigated by repeating the GAA treatment using a freshly prepared $NaBH_4$ solution. Continuous H_2 generation by using a continuous flow system was also done by using 0.1 ng CuNWs with 10 mL of 1 wt% $NaBH_4$. The continuous flow system was set up by using a syringe pump. $NaBH_4$ was pumped at three different flow rates (2.5, 1.3, and 0.8 mL h^{-1}) and passed through column reactor fitted on a HotCoil coil reactor (HotColumn™, Uniqsis, Cambridge, UK).

2.5. Characterization

The morphology of the CuNWs was analyzed by a field emission scanning electron microscope (FESEM, MERLIN ZEISS) and high-resolution transmission electron microscopy (HRTEM, FEI Technai G2 T20, Thermo Fisher, Waltham, MA, USA). The energy-dispersive X-ray (EDX) spectroscopy mapping was done by FESEM (FEI Quanta 400, Thermo Fisher). The chemical composition and crystal structure of the samples were examined by X-ray diffraction (XRD, Bruker D8 Advance) using Cu Kα radiation. The d-spacing (d) of the CuNWs was calculated using Bragg's equation $\lambda = 2d \sin\theta$, where λ is the wavelength of X-ray radiation used, θ is the peak position angle, and d is the inter-planer distance.

3. Results

3.1. Characterization of CuNWs

The characterization of CuNWs using FESEM and XRD can be found from our previous study [5], where it can be seen that high-aspect ratio CuNWs (~2600) were successfully synthesized from the hydrothermal reaction. Figure S1a presents the HRTEM image of a nanowire that shows the lattice fringe spacing of 0.21 nm which corresponds to the d-spacing value of the (111) planes of fcc Cu [39,40] and is consistent with the previous XRD result. Figure S1b shows the EDX mapping of the Cu contents on the cotton cloth. It can be seen that there were only trace amounts of Cu added onto the cloth; due to the small size of the CuNWs, they could not be seen clearly among the fibers of the cotton cloth.

3.2. H_2 Production

3.2.1. Effects of pH

The hydrolysis of $NaBH_4$ can be significantly influenced by the pH and temperature of the reaction. Compared with pure water, the hydrolysis of $NaBH_4$ in water-alkaline solution is much slower due to the *in situ* simultaneous hydrolysis of sodium metaborate ($NaBO_2$) which leads to the formation of NaOH, as shown in Equations (1) and (2) [41,42]:

$$NaBH_{4(aq)} + 2H_2O_{(l)} \rightarrow NaBO_{2(aq)} + 4H_{2(g)} \quad (1)$$

$$NaBO_{2(aq)} + 2H_2O_{(l)} \rightarrow NaOH_{(aq)} + H_3BO_{3(aq)} \quad (2)$$

The importance of pH makes it the first parameter tested in this study. Figure 1 shows the H_2 generation at three different pHs (10.45, 12, and 13). pH 10.45 was the initial value of the $NaBH_4$ solution without any adjustments. NaOH (0.1 M) was added to obtain pH 12 and pH 13. The H_2 generation at pH 10.45 and 12 was almost the same within the period of 240 min, meanwhile, at pH 13, the hydrolysis reaction was severely inhibited. This shows that H_2 generation can be greatly suppressed with the addition of alkali substances [43]. Table 1 shows the list of HGRs obtained from the hydrolysis of $NaBH_4$ at different pHs. It can be seen that the HGR value increased from pH 10.45 to 12, but decreased at pH 13. This is probably due to the involvement of OH^- in the hydrolysis of $NaBH_4$. The catalyzed hydrolysis of $NaBH_4$ can be accelerated with an appropriate increase in the NaOH concentration, thus enhancing the HGR. However, too much of NaOH could lead to a decrease in the solubility of $NaBO_2$, thus causing the subsequent precipitation from the solution, adherence on the surface of the catalyst, and blockage of the active sites [33,44]. This would then hinder the contact of BH_4^- with the catalyst surface, hence decreasing the hydrolysis rate [36]. With consideration of the real-life application in terms of the HGR, high H_2 capacity, and long shelf life of the fuel solution, pH 12 was chosen as the optimized pH of the $NaBH_4$ solution for further kinetics studies.

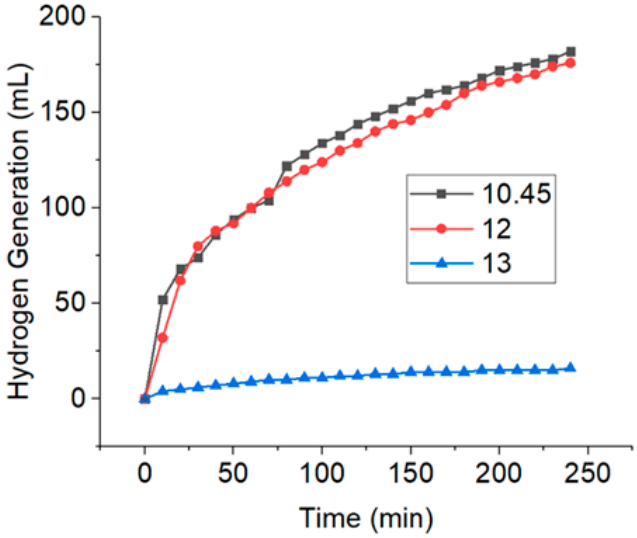

Figure 1. Plot of H_2 generation versus time on the effect of different pH (conditions: 0.1 ng CuNWs, 10 mL of [$NaBH_4$] = 1 wt%, and temperature = 298 K).

Table 1. List of H_2 generation rate (HGR) values on different pH values.

pH	HGR (mL min^{-1} g^{-1} $\times$ 10^{10})
10.45	2.38
12	2.7
13	0.1

3.2.2. Effects of Catalyst Loading

In the present study, CuNWs were investigated as a catalyst for H_2 generation from an alkaline $NaBH_4$ solution. Therefore, the effect of the CuNWs' loadings was tested. Figure 2a shows the plot of H_2 generation of different loadings of the catalyst with and without GAA treatment vs. time of reaction. It can be seen that there was very low H_2 generation without GAA treatment on the CuNWs strips. This is probably due to the presence of residual ODA and a thin oxide layer on the surface of the CuNWs [9], which would prevent the direct contact of reactants with the active sites of the CuNWs. Even though the H_2 generation using non-treated CuNWs strips was low, the total H_2 generation in 240 min was slightly higher (19 mL) in comparison with when no catalyst was added to the solution (13 mL). After the treatment with GAA, the H_2 generation increased significantly even with a very small amount of catalyst. This shows that the oxide and residual capping agent layers can be removed by using a short GAA treatment [45].

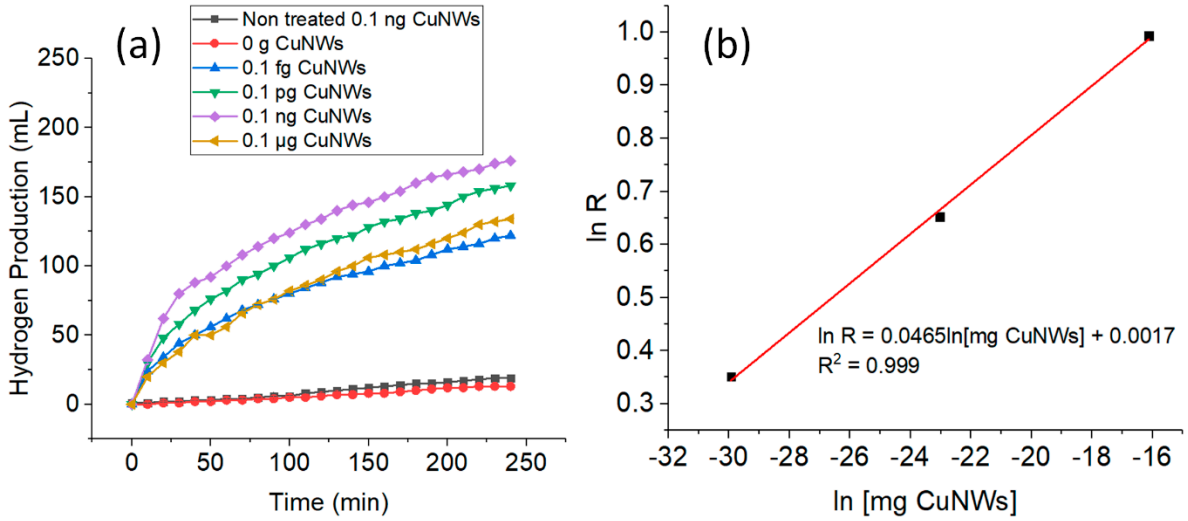

Figure 2. Plot of (**a**) different copper nanowires' (CuNWs) loadings on H_2 generation versus time; and (**b**) HGR versus CuNWs' loadings, both in logarithmic scale. (Conditions: 10 mL of [$NaBH_4$] = 1 wt%, pH = 12, and temperature = 298 K).

From Figure 2a, it can be seen that with the increase in catalyst loading (0–0.1 ng), the volume of H_2 generation increases as well. When there was no catalyst added, the volume of H_2 produced was only 13 mL in 240 min. According to the hydrolysis reactions, $NaBH_4$ reacts slowly with water even without a catalyst to generate H_2, even though it is not stable in air [43]. In comparison, when just a small amount of catalyst was added (0.1 fg), the volume of H_2 generation increased significantly. In 240 min, the hydrolysis of $NaBH_4$ for 0.1 fg, 0.1 pg, and 0.1 ng were 122, 158, and 176 mL, respectively. The enhancement in catalytic activity can be attributed to the increase in the specific surface area and more exposed active sites due to the addition of the CuNWs [17]. As the hydrolysis of $NaBH_4$ proceeded, the rate in H_2 generation started to decrease. During the hydrolysis process, the agglomeration of H_2 and blockage of the active sites could impede the formation of new active sites for further catalytic cycles [17]. When the catalyst loading increased to 0.1 µg, only 134 mL of H_2 gas was collected. This decrease in H_2 generation is probably due to the agglomeration of excess CuNWs which could inhibit some of the active sites [46]. The rate of H_2 generation was determined from the linear portion of each plot in Figure 2a. In this study, 0.1 ng was chosen as the fixed catalyst loading for the rest of the experiments due to easier handling and the volume of H_2 generation obtained after 240 min was the highest. The HGR obtained for this study by using 0.1 ng CuNWs is 2.7×10^{10}, and this value is ~3.27×10^7 times higher than a previously reported Cu-based catalyst [12]. This indicates the importance of GAA treatment on CuNWs before the catalytic hydrolysis process. Figure 2b shows the values of the HGR versus the initial loadings of the CuNWs, both in logarithmic scale. The slope of the

straight line is nearly zero (0.0465), indicating that the catalytic hydrolysis of $NaBH_4$ is approximately zero order with respect to the catalyst loadings.

Presently, the dissociative chemisorption of BH_4^- ions on the catalyst surface is generally accepted as the first kinetic step of the metal-catalyzed hydrolysis of $NaBH_4$ [34,47]. Holbrook and Twist [48] suggested that the H_2 was generated from both water and borohydride. Firstly, BH_4^- ions are adsorbed on the electron-enriched Cu active sites of the CuNWs. The Cu-BH_4^- ions then further dissociate to form Cu-BH_3^- and Cu-H intermediates (Equation (3)). Subsequently, Cu-BH_3^- reacts with H_2O, possibly via the BH_3 intermediate, to generate Cu-H and $BH_3(OH)^-$ (Equations (4)–(6)). After that, $BH_3(OH)^-$ undergoes a stepwise replacement of the B-H bonds by B-OH^-, which then finally yields $B(OH)_4^-$. Next, the Cu-H species combines with another Cu-H to afford H_2, and the active sites are regenerated (Equation (7)) [17,34].

$$2Cu + BH_4^- \leftrightarrow Cu\text{-}BH_3^- + Cu\text{-}H \quad (3)$$

$$Cu\text{-}BH_3^- \leftrightarrow BH_3 + Cu + e_{Cu}^- \quad (4)$$

$$BH_3 + OH^- \rightarrow BH_3(OH)^- \quad (5)$$

$$Cu + e_{Cu}^- + H_2O \leftrightarrow Cu\text{-}H + OH^- \quad (6)$$

$$Cu\text{-}H + Cu\text{-}H \rightarrow 2Cu + H_2 \quad (7)$$

3.2.3. Effects of Concentrations of $NaBH_4$

The effect of the initial $NaBH_4$ concentration on the hydrolysis was studied by employing 0.1 ng CuNWs in an ambient condition. Figure 3a shows that the total H_2 generation was 35, 90, 176, 250, and 162 mL by using 0.1, 0.5, 1, 3, and 5 wt% $NaBH_4$, respectively. It can be seen that by increasing the $NaBH_4$ concentration from 0.1 to 3 wt%, the H_2 generation increased as well. However, at the $NaBH_4$ concentration of 5 wt%, the volume of H_2 generation decreased to 162 mL. This can also be seen with the HGR of the different concentrations of $NaBH_4$ (Table 2), where the HGR increases with the increase in the $NaBH_4$ concentrations (0.1–3 wt%), and then decreases when 5 wt% of $NaBH_4$ is used. For the rest of the experiments, the $NaBH_4$ concentration of 1 wt% was chosen for economic reasons.

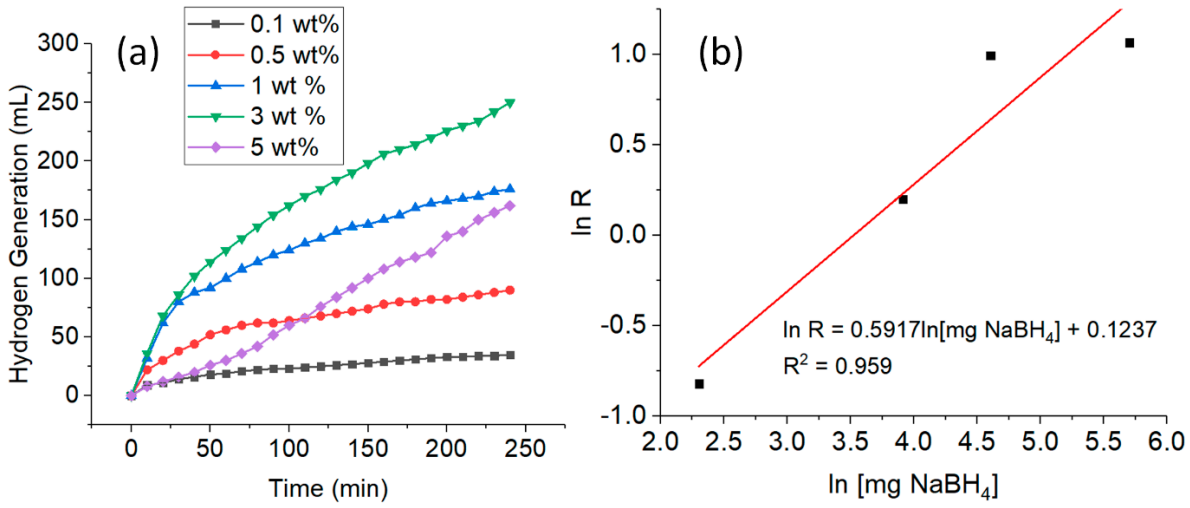

Figure 3. Plot of (**a**) different $NaBH_4$ concentrations (wt%) on H_2 generation versus time; and (**b**) HGR versus $NaBH_4$ concentrations, both in logarithmic scale. (Conditions: CuNWs = 0.1 ng, pH = 12, and temperature = 298 K).

Table 2. List of HGR values of different $NaBH_4$ concentrations.

Concentration of $NaBH_4$ (wt%)	HGR ($mLmin^{-1}g^{-1} \times 10^{10}$)
0.1	0.44
0.5	1.22
1	2.7
3	2.9
5	0.52

Theoretically, a higher concentration of $NaBH_4$ is desired to achieve a high capacity of H_2. Therefore, when the $NaBH_4$ concentration used is less than the highest HGR obtained, more H_2O and BH_4^- can be in contact with the active sites on the surface of the catalyst to generate H_2 at higher $NaBH_4$ concentrations. However, $NaBO_2$ was produced simultaneously with H_2. Due to the low solubility of $NaBO_2$ under alkaline solution, $NaBO_2$ accumulation on the surface of the catalyst and solution would occur at higher initial $NaBH_4$ concentrations [46,49,50] Consequently, this will increase the solution viscosity [46,51] and further retard the mass transfer and decrease the H_2 generation [33]. At higher concentrations of $NaBH_4$, the insufficient active sites for the target reaction contributed to the lower catalytic performance [46].

Figure 3b shows the values of the HGR versus the initial concentration of $NaBH_4$, both in logarithmic scale. The HGR in the catalytic hydrolysis of $NaBH_4$ was calculated from the slope of each plot in the initial linear portion. Based on the slope of the straight line, it is indicating that the catalytic hydrolysis of $NaBH_4$ is 0.59 order with respect to the concentrations of $NaBH_4$, suggesting that the reaction follows fractional order kinetics with $NaBH_4$ [42]. Consequently, the rate law of each catalyst for the catalytic hydrolysis of $NaBH_4$ in this study can be given as in Equation (8):

$$\frac{-4d[NaBH_4]}{dt} = \frac{d[H_2]}{dt} = k[CuNWs]^{0.05}[NaBH_4]^{0.59} \quad (8)$$

3.2.4. Effects of Temperature

Considering the fact that the reaction temperature is an important factor influencing the hydrolysis kinetics of $NaBH_4$, the effect of the reaction temperature was also investigated. Figure 4a shows the H_2 generation by using CuNWs as the catalyst at a temperature ranging from 298 to 333 K. It can be observed that the H_2 generation increases significantly with the reaction temperature. The time taken to reach a total volume of H_2 generation of 250 mL was 60, 30, and 9 min at 313, 323, and 333 K, respectively. At an elevated temperature, more active reacting molecules are available which caused the faster H_2 generation at a higher temperature [27].

The rate constants of H_2 generation from the hydrolysis were measured from the linear portions of the H_2 generation plots of the four different temperatures. These values were then used for the calculation of the activation energy (E_a) from the Arrhenius plot. Figure 4b shows the plot of the log scale of rate constant and inverse temperature. The activation energy of $NaBH_4$ hydrolysis catalyzed by CuNWs was determined from the Arrhenius equation (Equation (9)):

$$\ln k = \ln A - (E_a/RT) \quad (9)$$

where k is the reaction rate, A is the Arrhenius constant, E_a is the activation energy (kJ mol^{-1}), R is the gas constant, and T is the absolute temperature (K). According to the slope of the straight line, the E_a obtained was 42.48 kJ mol^{-1}. This value is comparable to the other values reported by using other non-noble metal-based catalysts (Table 3). The lower E_a of this study shows that a fast hydrolysis reaction rate was successfully achieved [14]. This indicates that CuNWs are a good and efficient catalyst for the hydrolysis of $NaBH_4$.

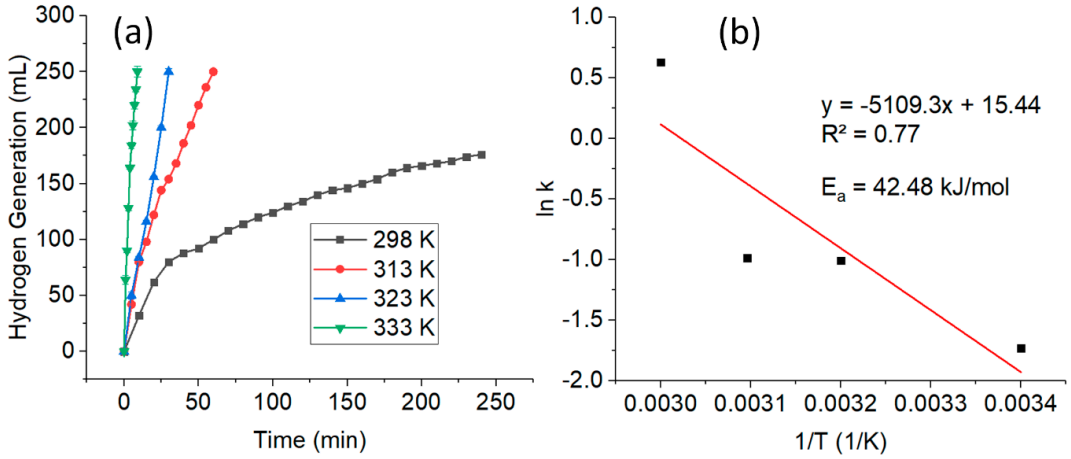

Figure 4. Plot of (**a**) different reaction temperatures on H_2 generation versus time; and (**b**) the Arrhenius plot, ln k versus 1/T. (Conditions: CuNWs = 0.1 ng, 10 mL of [$NaBH_4$] = 1 wt%, and pH = 12).

Table 3. List of comparisons of catalytic performance in this study with those reported in previous studies.

Catalyst	HGR ($mL\ min^{-1}\ g^{-1}$)	E_a ($kJ\ mol^{-1}$)	Reference
Cobalt/iron(II,III) oxide@carbon (Co/Fe_3O_4@C)	1403	49.2	[46]
Nickel-cobalt-boride (Ni–Co–B)	6400	33.1	[34]
Reduced graphene oxide-nickel (rGO-Ni)	33000	-	[52]
Silver/multi walled carbon nanotubes (Ag/MWCNT)	17.4	44.45	[53]
Palladium/multi walled carbon nanotubes (Pd/MWCNT)	23.0	62.66	[30]
Copper-ferum-boride (Cu-Fe-B)	-	57	[36]
Molybdenum disulfide/palm oil waste activated carbon (MoS_2/POAC)	1170.66	39.1	[54]
Cobalt-cerium-boride/chitosan-derived carbon (Co-Ce-B/Chi-C)	4760	33.1	[24]
Cobalt-molybdenum/three dimensional graphene oxide (Co-Mo/3DGO)	7023.3	35.6	[27]
Nickel-cobalt-phosphorus/γ-aluminium oxide (Ni-Co-P/γ-Al_2O_3)	5180	52.05	[50]
Cu based catalyst	825	61.16	[12]
Copper oxide/cobalt(II, III) oxide (CuO/Co_3O_4)	6162.55	56.38	[37]
CuNWs (0.1 ng)	2.7×10^{10}	42.48	This study

3.2.5. Reusability Test

The reusability of a catalyst is an important aspect to consider for stability, durability, and practical applications. Therefore, the reusability test of CuNWs as catalysts for the hydrolysis of $NaBH_4$ was studied under similar experimental conditions. Figure 5a,b shows the H_2 generation and HGR of the CuNWs without retreatment with GAA. By the second cycle, the catalytic performance of the CuNWs greatly decreased. In comparison with the first cycle where 176 mL of H_2 gas was collected in 240 min, the total volume of H_2 gas collected in the second cycle was only 16 mL. The volume of gas collected in the second cycle was only 9% of the initial cycle. This is probably due to the increase in boron products such as metaborate which hinder the accessibility of the active sites of the catalyst [36], thus decreasing its catalytic performance.

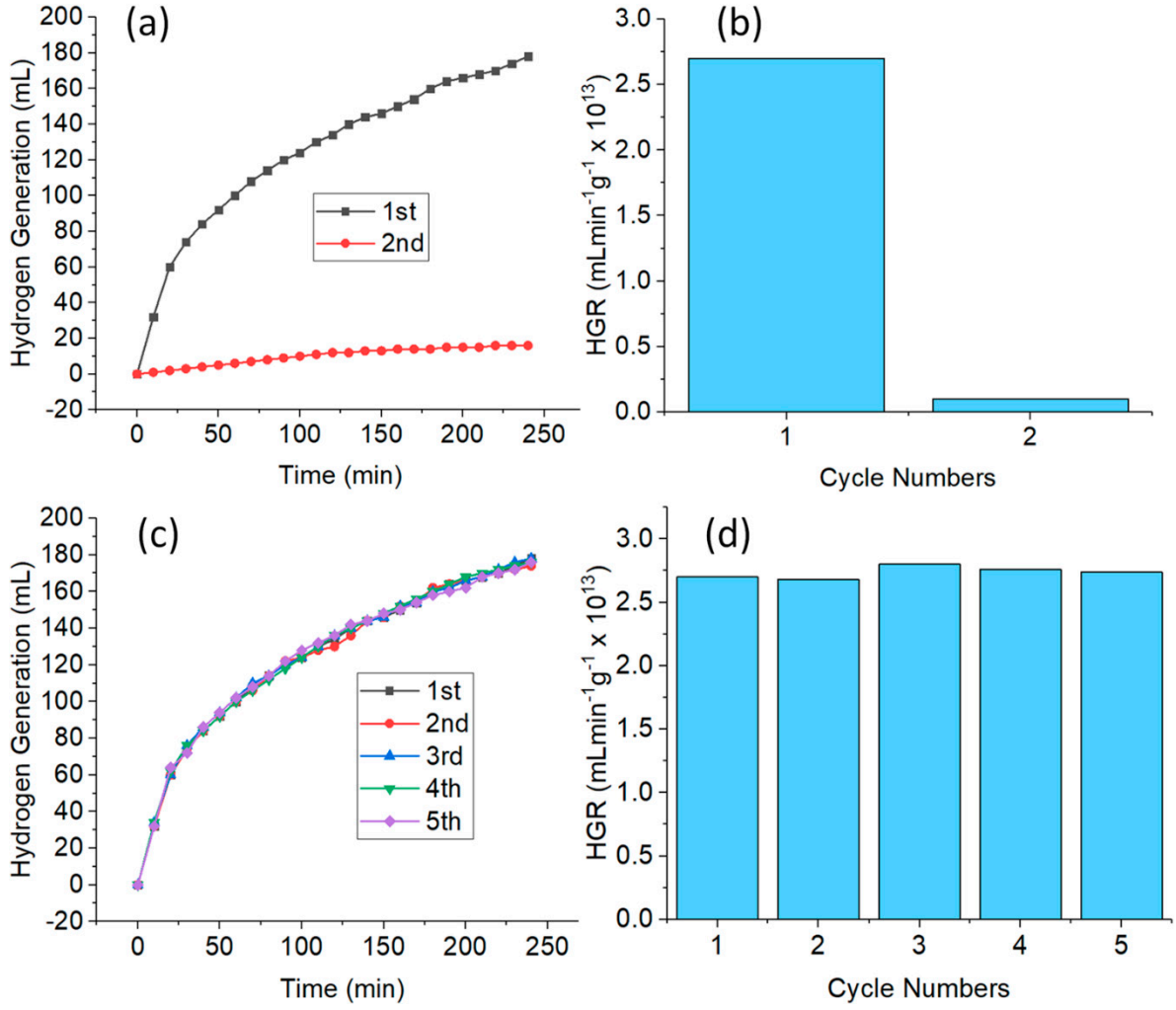

Figure 5. Plot of (**a**) H_2 generation versus time; and (**b**) HGR of the hydrolysis of $NaBH_4$ without retreatment of the CuNWs strips for two cycles, and (**c**) H_2 generation versus time; and (**d**) HGR of $NaBH_4$ with retreatment of the CuNWs using glacial acetic acid (GAA) in five consecutive cycles. (Conditions: CuNWs = 0.1 ng, 10 mL of [$NaBH_4$] = 1 wt%, pH = 12, and temperature = 298 K).

Due to the lower catalytic performance of the CuNWs in the second cycle of the $NaBH_4$ hydrolysis, the CuNWs strips were treated with GAA. Figure 5c,d shows the results of the reusability tests for the retreated CuNWs strips in five consecutive cycles. The volume of H_2 gas generation and the HGR were stable and consistent throughout the entire cycles without any noticeable differences. This efficient catalytic performance can be attributed to the good retention of the CuNWs on the cotton cloth which enabled the good recoverability of the CuNWs. Figure 6a,b shows the plot of the same CuNWs strip used as a catalyst for every week in a month. The total volume of H_2 generation and the HGR obtained in the span of a month were almost constant, which further shows the competence and stability of CuNWs as a catalyst in the hydrolysis of $NaBH_4$.

3.2.6. Catalytic Efficiency in Continuous Flow System

The key advantage of a continuous flow system is the ability to accurately control the reaction parameters for a scale-up laboratory reaction [55,56]. Hence, it is significant to measure the catalytic efficiency of the continuous flow system proposed. The experimental setup is illustrated in Figure 7. Table 4 shows the total production of H_2 obtained using the continuous flow system in the absence and presence of a catalyst at different flow rates. Based on Table 4, it can be seen that the H_2 production increased significantly with the presence of the CuNWs. When the flow rate decreased, the total

volume of H_2 increased, which can be attributed to the increased retention time of the $NaBH_4$ solution in contact with the CuNWs [57]. At the same time, the yield of H_2 increased with the decrease in the flow rate applied. The results show that CuNWs can catalyze the hydrolysis of $NaBH_4$ by using a continuous flow system. Table 5 lists the HGR for different production methods, showing the excellent catalytic performance of CuNWs in the production of H_2 gas.

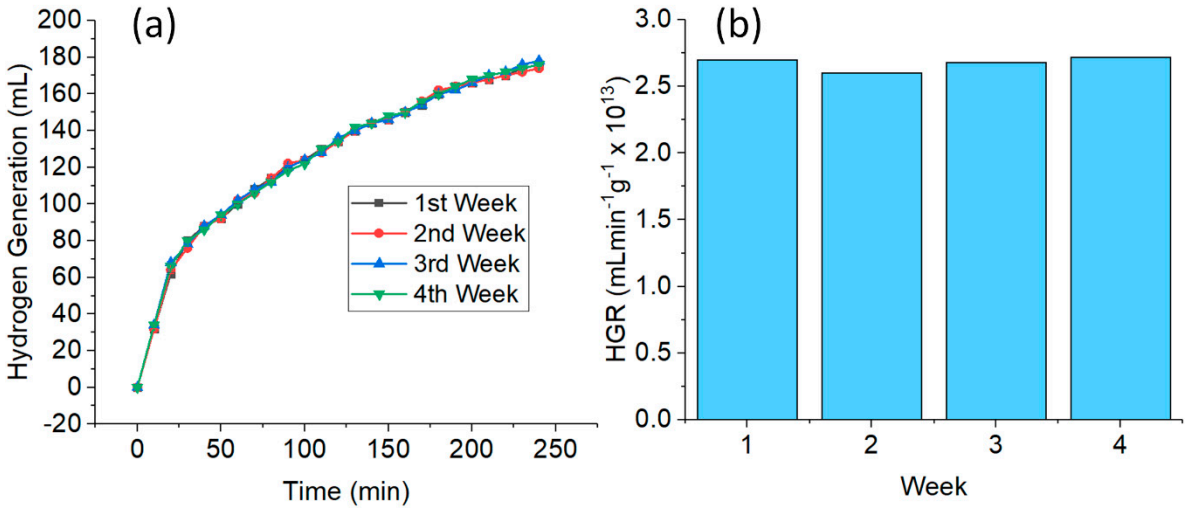

Figure 6. Plot of (**a**) H_2 generation versus time; and (**b**) HGR of the hydrolysis of $NaBH_4$ of the CuNWs strips for four weeks (conditions: CuNWs = 0.1 ng, 10 mL of [$NaBH_4$] = 1 wt%, pH = 12, and temperature = 298 K).

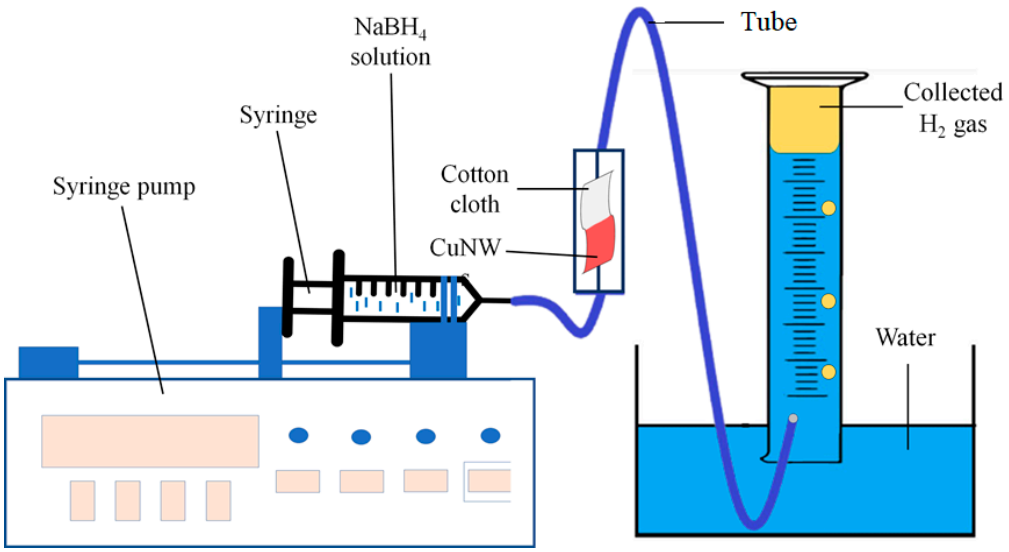

Figure 7. Schematic diagram of the continuous flow system setup for the production of H_2 (conditions: CuNWs = 0.1 ng, [$NaBH_4$] = 1 wt%, pH = 12, and temperature = 298 K).

Table 4. Total volume and yield of H_2 produced with different flow rates (with and without CuNWs).

Flow Rate (mL h^{-1})	Volume of H_2 in the Absence of CuNWs (mL)	Volume of H_2 in the Presence of CuNWs (mL)	Yield of H_2 in the Presence of CuNWs (%)
2.5	9	49	18.85
1.3	19	158	60.77
0.8	26	238	91.54

Table 5. Comparison of HGR using different processes.

Method	HGR (mmol h^{-1})	References
Photo-fermentation	0.16	[58]
Direct bio-photolysis	0.07	[59]
Photocatalysis (visible light irradiation)	0.048	[60]
Photocatalytic decomposition of ammonia borane	0.022	[61]
Batch hydrolysis of $NaBH_4$ [1]	1.8	This work
Continuous hydrolysis of $NaBH_4$ (flow rate = 0.8 mL h^{-1})	0.6	

[1] Conditions: CuNWs = 0.1 ng, [$NaBH_4$] = 1 wt%, pH = 12, and temperature = 298 K.

4. Conclusions

In this research work, a CuNWs catalyst was prepared by a simple hydrothermal method and used as a catalyst to produce H_2 from the hydrolysis of $NaBH_4$. An impressive catalytic performance was achieved by using a small amount (0.1 ng) of the catalyst, which yielded a high volume of H_2 and the HGR was obtained. Furthermore, a low E_a (42.48 kJ mol^{-1}) was calculated which shows the excellent catalytic activity of CuNWs. The effectiveness of the GAA treatment on the CuNWs before each reusability cycle was also shown. Consequently, the stable and consistent H_2 generation and HGR for the reusability test up to five cycles and stability test for four weeks suggests that CuNWs are a suitable catalyst for practical applications. The continuous production of H_2 could be a potential supply for proton-exchange membrane fuel cells.

Supplementary Materials: The following are available online at http://www.mdpi.com/2079-4991/10/6/1153/s1. Figure S1: HRTEM and EDX mapping of the CuNWs/CC sample.

Author Contributions: Conceptualization, A.S.H., M.A.N.M.N. and C.H.C.; methodology, A.S.H.; software, A.S.H.; validation, A.S.H., M.A.N.M.N. and C.H.C.; formal analysis, A.S.H.; writing—original draft preparation, A.S.; writing—review and editing, A.S.H. and C.H.C.; visualization, A.S.H. and M.A.N.M.N.; supervision, C.H.C., S.X.C. and S.Z.; project administration, C.H.C., S.X.C., P.S.K. and S.Z.; funding acquisition, C.H.C., S.X.C. and S.Z. All authors have read and agreed to the published version of the manuscript.

Funding: This research was funded by Universiti Kebangsaan Malaysia (DIP-2019-003) and The APC was funded by Universiti Kebangsaan Malaysia.

Acknowledgments: The authors would like to thank the Centre of Research and Instrumentation (CRIM), UKM for the research grant (DIP-2019-003) provided.

Conflicts of Interest: The authors declare no conflict of interest.

References

1. Lau, K.S.; Chin, S.X.; Tan, S.T.; Lim, F.S.; Chang, W.S.; Yap, C.C.; Jumali, M.H.H.; Zakaria, S.; Chook, S.W.; Chia, C.H. Silver nanowires as flexible transparent electrode: Role of PVP chain length. *J. Alloys Compd.* **2019**, *803*, 165–171.
2. Chook, S.W.; Chia, C.H.; Zakaria, S.; Neoh, H.M.; Jamal, R. Effective immobilization of silver nanoparticles on a regenerated cellulose-chitosan composite membrane and its antibacterial activity. *New J. Chem.* **2017**, *41*, 5061–5065. [CrossRef]
3. Chook, S.W.; Chia, C.H.; Kaco, H.; Zakaria, S.; Huang, N.M.; Neoh, H.M. Highly porous chitosan beads embedded with silver-graphene oxide nanocomposites for antibacterial application. *Sains Malays.* **2016**, *45*, 1663–1667.
4. Abdul Halim, N.H.; Lee, Y.H.; Marugan, R.S.P.M.; Hashim, U. Mediatorless impedance studies with titanium dioxide conjugated gold nanoparticles for hydrogen peroxide detection. *Biosensors* **2017**, *7*, 38. [CrossRef]
5. Hashimi, A.S.; Nohan, M.A.N.M.; Chin, S.X.; Zakaria, S.; Chia, C.H. Rapid catalytic reduction of 4-nitrophenol and clock reaction of methylene blue using copper nanowires. *Nanomaterials* **2019**, *9*, 936. [CrossRef]
6. Wei, N.; Wu, Y.; Wang, M.; Sun, W.; Li, Z.; Ding, L.; Cui, H. Construction of noble metal-free TiO2 nanobelt/ZnIn2S4 nanosheet heterojunction nanocomposite for highly efficient photocatalytic hydrogen evolution. *Nanotechnology* **2018**, *30*, 045701. [CrossRef]

7. Yang, L.; Wang, X.; Wang3, J.; Cui, G.; Liu, D. Graphite carbon nitride/boron doped graphene hybrid for efficient hydrogen generation reaction. *Nanotechnology* **2018**, *29*, 345705. [CrossRef]
8. Mohl, M.; Pusztai, P.; Kukovecz, A.; Konya, Z.; Kukkola, J.; Kordas, K.; Vajtai, R.; Ajayan, P.M. Low-temperature large-scale synthesis and electrical testing of ultralong copper nanowires. *Langmuir* **2010**, *26*, 16496–16502. [CrossRef]
9. Mayousse, C.; Celle, C.; Carella, A.; Simonato, J.-P. Synthesis and purification of long copper nanowires. Application to high performance flexible transparent electrodes with and without PEDOT:PSS. *Nano Res.* **2014**, *7*, 315–324. [CrossRef]
10. Jin, M.; He, G.; Zhang, H.; Zeng, J.; Xie, Z.; Xia, Y. Shape-controlled synthesis of copper nanocrystals in an aqueous solution with glucose as a reducing agent and hexadecylamine as a capping agent. *Angew. Chem. Int. Ed.* **2011**, *50*, 10560–10564. [CrossRef]
11. Sun, Y.; Xu, L.; Yin, Z.; Song, X. Synthesis of copper submicro/nanoplates with high stability and their recyclable superior catalytic activity towards 4-nitrophenol reduction. *J. Mater. Chem. A* **2013**, *1*, 12361–12370. [CrossRef]
12. Balbay, A.; Saka, C. Effect of phosphoric acid addition on the hydrogen production from hydrolysis of $NaBH_4$ with Cu based catalyst. *Energy Sources Part A Recover. Util. Environ. Eff.* **2018**, *40*, 794–804. [CrossRef]
13. Ouyang, L.; Zhong, H.; Li, H.-W.; Zhu, M. A recycling hydrogen supply system of $NaBH_4$ based on a facile regeneration process: A review. *Inorganics* **2018**, *6*, 10. [CrossRef]
14. Shi, L.; Xie, W.; Jian, Z.; Liao, X.; Wang, Y. Graphene modified Co–B catalysts for rapid hydrogen production from $NaBH_4$ hydrolysis. *Int. J. Hydrogen Energy* **2019**, *44*, 17954–17962. [CrossRef]
15. Abdul-Majeed, W.S.; Arslan, M.T.; Zimmerman, W.B. Application of acidic accelerator for production of pure hydrogen from $NaBH_4$. *Int. J. Ind. Chem.* **2014**, *5*, 15. [CrossRef]
16. Demirci, U.B.; Akdim, O.; Andrieux, J.; Hannauer, J.; Chamoun, R.; Miele, P. Sodium borohydride hydrolysis as hydrogen generator: Issues, state of the art and applicability upstream froma fuel cell. *Fuel Cells* **2010**, *10*, 335–350. [CrossRef]
17. Shi, L.; Chen, Z.; Jian, Z.; Guo, F.; Gao, C. Carbon nanotubes-promoted Co–B catalysts for rapid hydrogen generation via $NaBH_4$ hydrolysis. *Int. J. Hydrogen Energy* **2019**, *44*, 19868–19877. [CrossRef]
18. Cai, W.; Wang, H.; Jiao, L.; Wang, Y.; Zhu, M. Remarkable irreversible and reversible dehydrogenation of LiBH4 by doping with nanosized cobalt metalloid compounds. *Int. J. Hydrogen Energy* **2013**, *38*, 3304–3312. [CrossRef]
19. Sahiner, N.; Yasar, A.O.; Aktas, N. Dicationic poly(4-vinyl pyridinium) ionic liquid capsules as template for Co nanoparticle preparation and H_2 production from hydrolysis of $NaBH_4$. *J. Ind. Eng. Chem.* **2015**, *23*, 100–108. [CrossRef]
20. Ali, F.; Khan, S.B.; Asiri, A.M. Enhanced H_2 generation from $NaBH_4$ hydrolysis and methanolysis by cellulose micro-fibrous cottons as metal templated catalyst. *Int. J. Hydrogen Energy* **2018**, *43*, 6539–6550. [CrossRef]
21. Liu, B.H.; Li, Z.P. A review: Hydrogen generation from borohydride hydrolysis reaction. *J. Power Sources* **2009**, *187*, 527–534. [CrossRef]
22. Zhong, H.; Wang, H.; Liu, J.W.; Sun, D.L.; Fang, F.; Zhang, Q.A.; Ouyang, L.Z.; Zhu, M. Enhanced hydrolysis properties and energy efficiency of MgH_2-base hydrides. *J. Alloys Compd.* **2016**, *680*, 419–426. [CrossRef]
23. Kunowsky, M.; Weinberger, B.; Lamari Darkrim, F.; Suárez-García, F.; Cazorla-Amorós, D.; Linares-Solano, A. Impact of the carbonisation temperature on the activation of carbon fibres and their application for hydrogen storage. *Int. J. Hydrogen Energy* **2008**, *33*, 3091–3095. [CrossRef]
24. Zou, Y.; Yin, Y.; Gao, Y.; Xiang, C.; Chu, H.; Qiu, S.; Yan, E.; Xu, F.; Sun, L. Chitosan-mediated Co-Ce-B nanoparticles for catalyzing the hydrolysis of sodium borohydride. *Int. J. Hydrogen Energy* **2018**, *43*, 4912–4921. [CrossRef]
25. Semiz, L.; Abdullayeva, N.; Sankir, M. Nanoporous Pt and Ru catalysts by chemical dealloying of Pt-Al and Ru-Al alloys for ultrafast hydrogen generation. *J. Alloys Compd.* **2018**, *744*, 110–115. [CrossRef]
26. Duman, S.; Özkar, S. Ceria supported manganese(0) nanoparticle catalysts for hydrogen generation from the hydrolysis of sodium borohydride. *Int. J. Hydrogen Energy* **2018**, *43*, 15262–15274. [CrossRef]
27. Li, Y.; Hou, X.; Wang, J.; Feng, X.; Cheng, L.; Zhang, H.; Han, S. Co-Mo nanoparticles loaded on three–dimensional graphene oxide as efficient catalysts for hydrogen generation from catalytic hydrolysis of sodium borohydride. *Int. J. Hydrogen Energy* **2019**, *44*, 29075–29082. [CrossRef]

28. Uzundurukan, A.; Devrim, Y. Hydrogen generation from sodium borohydride hydrolysis by multi-walled carbon nanotube supported platinum catalyst: A kinetic study. *Int. J. Hydrogen Energy* **2019**, *44*, 17586–17594. [CrossRef]
29. Özkar, S.; Zahmakıran, M. Hydrogen generation from hydrolysis of sodium borohydride using Ru(0) nanoclusters as catalyst. *J. Alloys Compd.* **2005**, *404*, 728–731. [CrossRef]
30. Huff, C.; Long, J.M.; Heyman, A.; Abdel-Fattah, T. Palladium nanoparticle multiwalled carbon nanotube composite as catalyst for hydrogen production by the hydrolysis of sodium borohydride. *ACS Appl. Energy Mater.* **2018**, *1*, 4635–4640. [CrossRef]
31. Zabielaitė, A.; Balčiūnaitė, A.; Stalnionienė, I.; Lichušina, S.; Šimkūnaitė, D.; Vaičiūnienė, J.; Šimkūnaitė-Stanynienė, B.; Selskis, A.; Tamašauskaitė-Tamašiūnaitė, L.; Norkus, E. Fiber-shaped Co modified with Au and Pt crystallites for enhanced hydrogen generation from sodium borohydride. *Int. J. Hydrog. Energy* **2018**, *43*, 23310–23318. [CrossRef]
32. Gao, Z.; Ding, C.; Wang, J.; Ding, G.; Xue, Y.; Zhang, Y.; Zhang, K.; Liu, P.; Gao, X. Cobalt nanoparticles packaged into nitrogen-doped porous carbon derived from metal-organic framework nanocrystals for hydrogen production by hydrolysis of sodium borohydride. *Int. J. Hydrogen Energy* **2019**, *44*, 8365–8375. [CrossRef]
33. Nie, M.; Zou, Y.C.; Huang, Y.M.; Wang, J.Q. Ni-Fe-B catalysts for $NaBH_4$ hydrolysis. *Int. J. Hydrogen Energy* **2012**, *37*, 1568–1576. [CrossRef]
34. Guo, J.; Hou, Y.; Li, B.; Liu, Y. Novel Ni–Co–B hollow nanospheres promote hydrogen generation from the hydrolysis of sodium borohydride. *Int. J. Hydrogen Energy* **2018**, *43*, 15245–15254. [CrossRef]
35. Krishna, R.; Fernandes, D.M.; Dias, C.; Ventura, J.; Freire, C.; Titus, E. Facile synthesis of novel Co-B@Ni/RGO nanocomposite: A cost effective catalyst for improved hydrogen generation with enhanced electrochemical activity. *Int. J. Hydrogen Energy* **2016**, *41*, 11498–11509. [CrossRef]
36. Loghmani, M.H.; Shojaei, A.F.; Khakzad, M. Hydrogen generation as a clean energy through hydrolysis of sodium borohydride over Cu-Fe-B nano powders: Effect of polymers and surfactants. *Energy* **2017**, *126*, 830–840. [CrossRef]
37. Xie, L.; Wang, K.; Du, G.; Asiri, A.M.; Sun, X. 3D hierarchical CuO/Co_3O_4 core-shell nanowire array on copper foam for on-demand hydrogen generation from alkaline $NaBH_4$ solution. *RSC Adv.* **2016**, *6*, 88846–88850. [CrossRef]
38. Seven, F.; Sahiner, N. Superporous P(2-hydroxyethyl methacrylate) cryogel-M (M:Co, Ni, Cu) composites as highly effective catalysts in H_2 generation from hydrolysis of $NaBH_4$ and NH_3BH_3. *Int. J. Hydrogen Energy* **2014**, *39*, 15455–15463. [CrossRef]
39. Zhao, Y.; Zhang, Y.; Li, Y.; Yan, Z. Soft synthesis of single-crystal copper nanowires of various scales. *New J. Chem.* **2012**, *36*, 130–138. [CrossRef]
40. Zhao, Y.; Zhang, Y.; Li, Y.; He, Z.; Yan, Z. Rapid and large-scale synthesis of Cu nanowires via a continuous flow solvothermal process and its application in dye-sensitized solar cells (DSSCs). *RSC Adv.* **2012**, *2*, 11544–11551. [CrossRef]
41. Minkina, V.G.; Shabunya, S.I.; Kalinin, V.I.; Martynenko, V.V.; Smirnova, A.L. Stability of alkaline aqueous solutions of sodium borohydride. *Int. J. Hydrogen Energy* **2012**, *37*, 3313–3318. [CrossRef]
42. Al-Thabaiti, S.A.; Khan, Z.; Malik, M.A. Bimetallic Ag-Ni nanoparticles as an effective catalyst for hydrogen generation from hydrolysis of sodium borohydride. *Int. J. Hydrogen Energy* **2019**, *44*, 16452–16466. [CrossRef]
43. Moon, G.Y.; Lee, S.S.; Lee, K.Y.; Kim, S.H.; Song, K.H. Behavior of hydrogen evolution of aqueous sodium borohydride solutions. *J. Ind. Eng. Chem.* **2008**, *14*, 94–99. [CrossRef]
44. Loghmani, M.H.; Shojaei, A.F. Hydrogen generation from hydrolysis of sodium borohydride by cubic Co-La-Zr-B nano particles as novel catalyst. *Int. J. Hydrogen Energy* **2013**, *38*, 10470–10478. [CrossRef]
45. Zhang, T.; Daneshvar, F.; Wang, S.; Sue, H.J. Synthesis of oxidation-resistant electrochemical-active copper nanowires using phenylenediamine isomers. *Mater. Des.* **2019**, *162*, 154–161. [CrossRef]
46. Chen, B.; Chen, S.; Bandal, H.A.; Appiah-Ntiamoah, R.; Jadhav, A.R.; Kim, H. Cobalt nanoparticles supported on magnetic core-shell structured carbon as a highly efficient catalyst for hydrogen generation from $NaBH_4$ hydrolysis. *Int. J. Hydrogen Energy* **2018**, *43*, 9296–9306. [CrossRef]
47. Dai, H.B.; Liang, Y.; Wang, P. Effect of trapped hydrogen on the induction period of cobalt-tungsten-boron/nickel foam catalyst in catalytic hydrolysis reaction of sodium borohydride. *Catal. Today* **2011**, *170*, 27–32. [CrossRef]

48. Holbrook, K.A.; Twist, P.J. Hydrolysis of the borohydride ion catalysed by metal-boron alloys. *J. Chem. Soc. A Inorg. Phys. Theor. Chem.* **1971**, 890–894. [CrossRef]
49. Xi, P.; Chen, F.; Xie, G.; Ma, C.; Liu, H.; Shao, C.; Wang, J.; Xu, Z.; Xu, X.; Zeng, Z. Surfactant free RGO/Pd nanocomposites as highly active heterogeneous catalysts for the hydrolytic dehydrogenation of ammonia borane for chemical hydrogen storage. *Nanoscale* **2012**, *4*, 5597–5601. [CrossRef]
50. Li, Z.; Li, H.; Wang, L.; Liu, T.; Zhang, T.; Wang, G.; Xie, G. Hydrogen generation from catalytic hydrolysis of sodium borohydride solution using supported amorphous alloy catalysts (Ni-Co-P/γ-Al2O3). *Int. J. Hydrog. Energy* **2014**, *39*, 14935–14941. [CrossRef]
51. Jeong, S.U.; Kim, R.K.; Cho, E.A.; Kim, H.J.; Nam, S.W.; Oh, I.H.; Hong, S.A.; Kim, S.H. A study on hydrogen generation from $NaBH_4$ solution using the high-performance Co-B catalyst. *J. Power Sources* **2005**, *144*, 129–134. [CrossRef]
52. Hostert, L.; Neiva, E.G.C.; Zarbin, A.J.G.; Orth, E.S. Nanocatalysts for hydrogen production from borohydride hydrolysis: Graphene-derived thin films with Ag and Ni-based nanoparticles. *J. Mater. Chem. A* **2018**, *6*, 22226–22233. [CrossRef]
53. Huff, C.; Long, J.M.; Aboulatta, A.; Heyman, A.; Abdel-Fattah, T.M. Silver nanoparticle/multi-walled carbon nanotube composite as catalyst for hydrogen production. *ECS J. Solid State Sci. Technol.* **2017**, *6*, 115–118. [CrossRef]
54. Rambabu, K.; Hai, A.; Bharath, G.; Banat, F.; Show, P.L. Molybdenum disulfide decorated palm oil waste activated carbon as an efficient catalyst for hydrogen generation by sodium borohydride hydrolysis. *Int. J. Hydrogen Energy* **2019**, *44*, 14406–14415. [CrossRef]
55. Watts, P.; Wiles, C. Micro reactors, flow reactors and continuous flow synthesis. *J. Chem. Res.* **2012**, *36*, 181–193. [CrossRef]
56. Watts, P. Continuous flow reactor technology for nanomaterial synthesis. *J. Biochips Tissue Chips* **2015**, *5*, 1.
57. Zhang, S.; Zhang, H.; Ni, T.; Shen, X. Highly efficient Au nanocatalysts for heterogeneous continuous-flow reactions using hollow CeO_2 microspheres as a functional skeleton. *Ind. Eng. Chem. Res.* **2018**, *57*, 3575–3582. [CrossRef]
58. Polle, J.E.W.; Kanakagiri, S.; Jin, E.S.; Masuda, T.; Melis, A. Truncated chlorophyll antenna size of the photosystems—A practical method to improve microalgal productivity and hydrogen production in mass culture. *Int. J. Hydrogen Energy* **2002**, *27*, 1257–1264. [CrossRef]
59. Nikolaidis, P.; Poullikkas, A. A comparative overview of hydrogen production processes. *Renew. Sustain. Energy Rev.* **2017**, *67*, 597–611. [CrossRef]
60. Lin, H.Y.; Shih, C.Y. Efficient one-pot microwave-assisted hydrothermal synthesis of M (M = Cr, Ni, Cu, Nb) and nitrogen co-doped TiO2 for hydrogen production by photocatalytic water splitting. *J. Mol. Catal. A Chem.* **2016**, *411*, 128–137. [CrossRef]
61. Jo, S.; Verma, P.; Kuwahara, Y.; Mori, K.; Choi, W.; Yamashita, H. Enhanced hydrogen production from ammonia borane using controlled plasmonic performance of Au nanoparticles deposited on TiO2. *J. Mater. Chem. A* **2017**, *5*, 21883–21892. [CrossRef]